

NOMA-Based Hybrid Satellite-UAV-Terrestrial Networks for Beyond 5G Maritime Internet of Things

Xinran Fang, Wei Feng, *Senior Member, IEEE*, Yanmin Wang, Yunfei Chen, *Senior Member, IEEE*, and Ning Ge, *Member, IEEE*

Abstract—Current fifth-generation (5G) networks do not cover the maritime area, causing difficulties in developing maritime Internet of Things (IoT). To tackle this problem, we establish a nearshore network by collaboratively using on-shore terrestrial base stations (TBSs) and tethered unmanned aerial vehicles (UAVs). These TBSs and UAVs form virtual clusters in a user-centric manner. Within each virtual cluster, non-orthogonal multiple access (NOMA) is adopted for agilely including various maritime IoT devices, which are usually sparsely distributed on the vast ocean. The nearshore network also shares spectrum with marine satellites. In such a NOMA-based hybrid satellite-UAV-terrestrial network, interference among different network segments, different clusters, as well as different users occurs. We thereby formulate a joint power allocation problem to maximize the sum rate of the network. Different from existing studies, we use large-scale channel state information (CSI) only for optimization to reduce system overhead. The large-scale CSI is obtained by using the position information of maritime IoT devices. The problem is non-convex with intractable non-linear constraints. We tackle these difficulties by adopting the relaxation methods, max-min optimization and the successive convex approximation technique. An iterative power allocation algorithm is accordingly proposed, which is shown effective for coverage enhancement by simulations. This shows the potential of NOMA-based hybrid satellite-UAV-terrestrial networks for maritime on-demand coverage.

Index Terms—Hybrid satellite-UAV-terrestrial network, interference, maritime Internet of Things, non-orthogonal multiple access (NOMA), power allocation.

I. INTRODUCTION

Nowadays, the fast development of maritime economies fosters maritime Internet of Things (IoT), emerging huge demand for maritime communications. Although the advanced fifth-generation (5G) techniques bring much convenience to the ground network, it still cannot support the efficient coverage on the sea. At present, maritime communication system mainly consists of two parts, the terrestrial base stations (TBSs) and the marine satellites. TBSs have limited coverage while satellites usually have low data rate and long transmission delay, thus the communication on the sea is far from satisfying.

X. Fang, W. Feng, and N. Ge are with the Beijing National Research Center for Information Science and Technology, Department of Electronic Engineering, Tsinghua University, Beijing 100084, China (e-mail: fxr20@mails.tsinghua.edu.cn, fengwei@tsinghua.edu.cn, geng@tsinghua.edu.cn).

Y. Wang is with the China Academy of Electronics and Information Technology, Beijing 100041, China (e-mail: yanmin-226@163.com).

Y. Chen is with the School of Engineering, University of Warwick, Coventry CV4 7AL, U.K. (e-mail: Yunfei.Chen@warwick.ac.uk).

How to construct an effective maritime network is still an open problem.

Generally speaking, although the satellite is a widely recognized way to achieve global coverage, it is more efficient to rely on the advanced terrestrial techniques to offer services for nearshore areas [1]. Note that the user distribution is uneven on the sea, and most communication demand happens within the exclusive economic zones (EEZs). Taking the ship distribution as an example, it is reported by the European Union that the coastal shipping takes 60% of all maritime goods transportation [2]. In this sense, a wide-band nearshore network is required to have adequate abilities for service supplies. However, TBSs should be deployed on the high lands or mountains to overcome the influence of the earth curvature [3], where the basic infrastructures such as optical fibers and power supply stations are hard to be deployed. The site limitations make it hard to densely deploy TBSs like the terrestrial cellular settings. Relying on TBSs only may not satisfy the pressing demand near the shore. To address these challenges, the recent rising technique of unmanned aerial vehicle (UAV) communications is promising to enhance the nearshore network [4]. By leveraging the manipulation of tethered UAVs, we may deploy them free from the ground conditions, and thus, alleviate the site problem of conventional TBSs. Due to the generally higher altitude, UAVs can provide wider coverage and better channels than TBSs [5], [6]. The TBS-UAV coordination can be designed so as to extend the efficient terrestrial services farther from the shore.

In practice, maritime IoT devices are widely and sparsely distributed [7]. The users that are relatively far from the coastline are traditionally poorly served by terrestrial facilities due to the severe signal attenuation of long-distance transmissions. To accommodate the wide sparsity of the maritime IoT and agilely take care of different users, the non-orthogonal multiple access (NOMA) transmission scheme can be considered for the nearshore network [8], [9]. On the one hand, this scheme is designed to serve a group of users within one resource block, thus more connections and higher spectrum efficiency can be achieved compared with the traditional orthogonal multiple access (OMA) method [10], [11]. On the other hand, NOMA could implement the successive interference cancellation (SIC) to extract the far users' interference from the near users' signals [12]. So, the far users can be better taken care of with more power allocated without causing much influence to the near users.

Similar to the terrestrial case, the spectrum scarcity problem also exists on the sea. To alleviate it, the nearshore network could share spectrum with marine satellites. We believe such a NOMA-based hybrid satellite-UAV-terrestrial network is promising to extend 5G to the ocean [4]. Nevertheless, it also faces unique challenges. Due to the geographical limitation of both deploying TBSs and dispatching tethered UAVs, the nearshore network is irregular, leading to complicated co-channel interference. Besides, the distinct covering abilities of TBSs, UAVs and satellites also cause multi-tier interference. In this work, we tackle these problems, so as to show the potential gain of NOMA-based hybrid satellite-UAV-terrestrial network for maritime coverage enhancement. Particularly, we exploit the unique feature of maritime communication channels and maritime users, and accordingly design a joint resource allocation scheme to maximize the sum rate of the system with practical constraints including affordable system overhead and low computational complexity.

A. Related Works

To the best of our knowledge, there are only few studies using UAVs for the coverage enhancement on the sea. To improve the rate of a target maritime user, Li *et al.* [13] leveraged a fix-wing UAV to provide dynamic coverage and jointly optimized UAV's trajectory and power. Wang *et al.* [14] extended the scenario to a multi-UAV case and proposed an on-demand coverage scheme to fairly serve nearshore users. Zhang *et al.* [15] utilized the UAV as a relay and optimized its placement to extend the coverage of the TBS. In addition, as for the cases with only TBSs and satellites, Wei *et al.* [1] utilized the maritime environment information to estimate the channel state and optimized the input covariance of TBSs to maximize the ergodic sum capacity. Xiao *et al.* [16] devised a voyage-based cooperative resource allocation scheme to reduce the system power consumption. These studies provide valuable references for the improvement of hybrid maritime networks. But none of them takes the wide sparsity of maritime IoT into account and the corresponding cooperative coverage scheme is still missing.

Beyond the maritime settings, some studies investigated the UAV-assisted hybrid architecture. As a representative example, Hua *et al.* [17] considered a UAV-aided cognitive satellite-terrestrial system and jointly optimized the trajectory and transmit power of a UAV to maximize the user rate. For the reduced cases of air-ground coordination, Zhao *et al.* [18] applied the NOMA technique to support massive connections and mitigated the bilateral interference between ground and UAV users. Peng *et al.* [19] alternately optimized the user scheduling and UAV's trajectory with the interference constraint of terrestrial NOMA users. These studies have demonstrated the great potentials of UAVs in different communication scenarios. However, in most practice, the UAV will not stand alone. The achievable performance gain of UAVs should be reexamined for the hybrid case.

When taking the systematical design into account, the cooperative resource allocation can be applied for interference mitigation. Liu *et al.* [20] proposed a process-oriented optimization framework to jointly allocate subchannels, transmit

power and hovering time of a UAV swarm. With the assistance of the NOMA technique, Lin *et al.* [21] utilized collaborative beamforming and power allocation to maximize the sum rate. Wang *et al.* [22] maximized the energy efficiency, and dedicated beamforming was applied to reduce the inter-user interference. Although these studies provide useful guidelines for interference mitigation in the hybrid network, most of them assume that the full channel state information (CSI) can be acquired for the optimization while ignoring the overhead problem. The cost efficiency should be considered from a practical perspective.

To construct a wide-band nearshore network, the tethered UAVs can be applied for coverage enhancement. But few studies give detailed regimes on how to integrate UAVs into maritime networks. In addition, the wide sparsity of maritime IoT requires on-demand coverage for different users. In this case, the performance of NOMA technique remains to be evaluated. Taking the harsh maritime environment into account, the acquisition of full CSI in the hybrid satellite-UAV-terrestrial network is challenging. It not only requires the inter-connection of space, air and ground network components but also faces outdated feedback due to the long delay of satellites. At the cost of huge overhead to acquire only inaccurate information is not an advisable choice in practice. In a nutshell, there still lack studies on the NOMA-based hybrid satellite-UAV-terrestrial network for the maritime IoT towards the on-demand coverage regime.

B. Main Contributions

In this paper, we explore the potential gain of NOMA-based hybrid satellite-UAV-terrestrial network for maritime coverage enhancement, using the unique feature of maritime channels and maritime users. We summarize our main contributions as follows.

- 1) We establish a hybrid maritime network for on-demand coverage, where the tethered UAVs are dispatched and form virtual clusters with TBSs, serving maritime IoT devices in a user-centric manner. Within each cluster, the NOMA technique is adopted for agilely including various IoT devices, so as to accommodate the wide sparsity of the maritime users. Out of the scope of the nearshore network, the marine satellites are utilized to provide additional connections. Taking the spectrum scarcity into account, we consider that the nearshore network shares spectrum with marine satellites.
- 2) We formulate a sum rate maximization problem with the constraints of inter-segment interference and the minimal quality-of-service (QoS) requirements. To reduce system overhead, only large-scale CSI is assumed available for the optimization, since it can be obtained based on the position information of maritime IoT devices. The formulated problem is non-convex with intractable non-linear constraints. We propose two relaxation methods to eliminate the fixed points in the constraints and derive an optimization-friendly max-min problem afterwards. Based on the method of successive convex approximation, the problem is solved in an efficient iterative way.

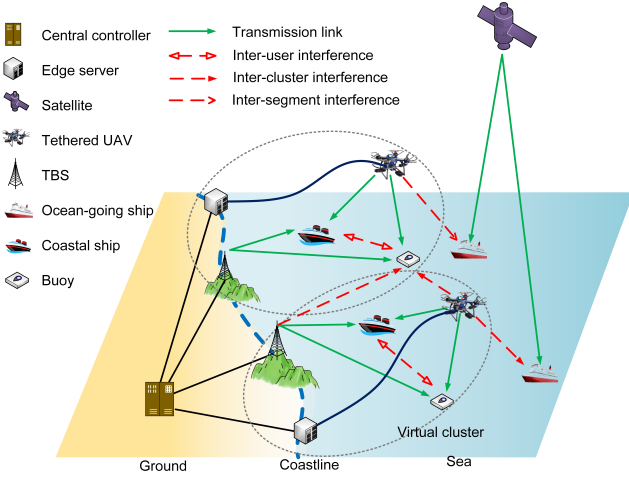


Fig. 1. Illustration of a NOMA-based hybrid satellite-UAV-terrestrial network on the ocean, where TBSs and UAVs form virtual clusters in a user-centric manner, and the coastal ship and buoy are paired in each virtual cluster. The ocean-going ships are connected by the satellite. In this network, there exists challenging inter-user, inter-cluster and inter-segment interference.

- 3) We propose a joint power allocation scheme. Simulation results show that its computational complexity is low. Besides, it can effectively mitigate the challenging inter-user, inter-cluster and inter-segment interferences within the hybrid network. We also show the potential gain of NOMA-based hybrid satellite-UAV-terrestrial network. It is observed that the nearshore network can be enhanced by UAVs, and NOMA can accommodate the wide sparsity of maritime users.

C. Organization and Notation

The rest of this paper is organized as follows. Section II introduces the system model of maritime hybrid satellite-UAV-terrestrial networks. The joint power allocation problem is investigated in Section III for maximizing the sum rate of the system with practical constraints. Simulation results and conclusions are presented in Section IV and Section V, respectively.

Throughout this paper, vectors and matrices are represented by lower and upper boldface symbols. $\mathbb{C}^{M \times N}$ represents the set of $M \times N$ complex matrices and \mathbf{I}_M is the unit matrix of $M \times M$. $\|\cdot\|$ denotes the Euclidean norm and $(\cdot)^H$ is the operation of transpose conjugate, $\det(\cdot)$ represents the determinant operator. The complex Gaussian distribution with zero mean and σ^2 variance is denoted as $\mathcal{CN}(0, \sigma^2)$. $\mathbb{E}_s(\cdot)$ is the expectation operation with respect to s .

II. SYSTEM MODEL

As shown in Fig. 1, we consider a NOMA-based satellite-UAV-terrestrial network on the sea. In the nearshore areas, the tethered UAVs are dynamically dispatched and form virtual clusters with TBSs for serving the users therein. When the virtual clusters are formed, we assume the positions of UAVs are fixed. These clusters can alleviate the site limitation of TBSs and also extend the coverage scope of the nearshore

network. There are multiple users in a cluster and different user pairs are allocated with orthogonal physical resource blocks (PRBs). Since the interference only occurs among the users using the same PRB, we thereby take one PRB and the users therein into account. As a common case, the paired users on the sea could be the coastal ships requiring high rate with the low-end devices like buoys requiring relatively low rate. In this sense, NOMA is suitable to offer high-rate services for the coastal ships while carrying additional bits for the buoys. As for the areas out of the coverage of the nearshore network, the marine satellites provide additional connections. To facilitate the systematic collaboration, inter-cluster connected edge servers are applied to collect position information and provide power supply for tethered UAVs. The central controller is responsible for the cooperative resource allocation.

To facilitate the problem formulation, we assume there are K virtual clusters and in cluster k ($k = 1, \dots, K$), two NOMA users equipped with M_k antennas are served by T_k TBSs and U_k UAVs. All TBSs and UAVs are set to have a single antenna. We also assume there are J satellite users in this system.

We consider a composite channel model to depict both the small-scale and the large-scale channel fading. Denote $\mathbf{H}_m^{(k,i)} \in \mathbb{C}^{M_k \times (T_i + U_i)}$ ($m = 1, 2, k, i = 1, \dots, K$) as the channel between user m in cluster k and transmitters in cluster i . It is given by

$$\mathbf{H}_m^{(k,i)} = \mathbf{S}_m^{(k,i)} (\mathbf{L}_m^{(k,i)})^{\frac{1}{2}} \quad (1)$$

where $\mathbf{S}_m^{(k,i)} \in \mathbb{C}^{M_k \times (T_i + U_i)}$ is the matrix of small-scale fading whose entries are independent and identically distributed (i.i.d) Gaussian random variables with $\mathcal{CN}(0, 1)$, $\mathbf{L}_m^{(k,i)} \in \mathbb{C}^{(T_i + U_i) \times (T_i + U_i)}$ denotes the large-scale fading. The matrix $\mathbf{L}_m^{(k,i)}$ is diagonal and we have

$$\mathbf{L}_m^{(k,i)} = \begin{bmatrix} l_{m,1}^{(k,i)} & & \mathbf{O} \\ & \ddots & \\ \mathbf{O} & & l_{m,T_i+U_i}^{(k,i)} \end{bmatrix} \quad (2)$$

where $l_{m,n}^{(k,i)}$ ($n = 1, \dots, T_i$) represents the large-scale fading of the TBS link and $l_{m,n}^{(k,i)}$ ($n = T_i + 1, \dots, T_i + U_i$) represents the large-scale fading of the UAV link. For the TBS link, we adopt the Hata propagation model according to paper [23]. Considering the antenna gains of TBSs, i.e. g_t , the total signal attenuation from TBS transmitter to receiver is calculated by

$$\begin{aligned} l_{m,n}^{(k,i)} [\text{dB}] = & g_t [\text{dBi}] + (44.9 - 6.55 \log_{10} h_t) \log_{10} \frac{d_{m,n}^{(k,i)}}{1000} \\ & + (35.46 - 1.1h_r) \log_{10} f_c - 13.82 \log_{10} h_r \\ & + 0.7h_r + C + 45.5 \end{aligned} \quad (3)$$

where $h_r(\text{m})$ and $h_t(\text{m})$ represent the height of user terminals and TBSs, $d_n^{(k,i)}(\text{m})$ is the distance element, $f_c(\text{MHz})$ is the carrier frequency and C is a constant related to the environment. For UAV channels, a model which considers both line-of-sight (LOS) and non-line-of-sight (NLOS) factors is

adopted [24]. With the antenna gains of UAVs, i.e., g_t , $l_n^{(k,i)}$ ($n = T_i + 1, \dots, T_i + U_i$) is calculated by

$$l_{m,n}^{(k,i)} [\text{dB}] = g_t [\text{dBi}] + \frac{A}{1 + ae^{-b(\rho_{m,n}^{(k,i)} - a)}} + B_{m,n}^{(k,i)} \quad (4)$$

where

$$A = \eta_{LOS} - \eta_{NLOS}, \quad (5a)$$

$$B_{m,n}^{(k,i)} = 20 \log_{10}(d_{m,n}^{(k,i)}) + 20 \log_{10}\left(\frac{4\pi f_c}{c}\right) + \eta_{NLOS}, \quad (5b)$$

$$\rho_{m,n}^{(k,i)} = \frac{180}{\pi} \arcsin\left(\frac{h_u}{d_{m,n}^{(k,i)}}\right) \quad (5c)$$

and $h_u(m)$ is the height of UAVs, c is the speed of light, η_{LOS} , η_{NLOS} , a , b are constants related to the environment. For further formulation, we transform $l_{m,n}^{(k,i)}$ from dB form as

$$l_{m,n}^{(k,i)} = 10^{-\frac{l_{m,n}^{(k,i)} [\text{dB}]}{10}}, m = 1, 2, k, i = 1, \dots, K. \quad (6)$$

Similarly, the channel of satellite users is given by

$$\mathbf{h}'^{(j,k)} = \mathbf{s}'^{(j,k)} (\mathbf{L}'^{(j,k)})^{\frac{1}{2}}, j = 1, \dots, J, k = 1, \dots, K \quad (7)$$

where $\mathbf{s}'^{(j,k)} \in \mathbb{C}^{1 \times (T_k + U_k)}$ denotes the small-scale fading and $\mathbf{L}'^{(j,k)} \in \mathbb{C}^{(T_k + U_k) \times (T_k + U_k)}$ is the large-scale fading, i.e., $\mathbf{L}'^{(j,k)} = \text{diag}\{l_1'^{(j,k)}, \dots, l_{T_k + U_k}'^{(j,k)}\}$.

From the expression of (3) and (4), it is easy to find that the large-scale fading is highly related to user and transmitter positions while the small-scale fading is unpredictable. To avoid the huge system overhead, we assume only large-scale CSI is available for optimization. The corresponding position data is collected by the edge servers from existing monitoring systems like the Automatic Identification System (AIS) [25] and the maritime map.

III. JOINT POWER ALLOCATION FOR SUM RATE MAXIMIZATION

A. Problem Formulation

Denote $\mathbf{x}^{(k)} \in \mathbb{C}^{(T_k + U_k) \times 1}$ as the downlink signal in cluster k ($k = 1, \dots, K$), and it is expressed as

$$\mathbf{x}^{(k)} = \mathbf{x}_1^{(k)} + \mathbf{x}_2^{(k)} \quad (8)$$

with $\mathbf{x}_1^{(k)}$, $\mathbf{x}_2^{(k)}$ representing the transmit signals of user 1 and user 2. The received signals can be given by

$$\mathbf{y}_1^{(k)} = \mathbf{H}_1^{(k,k)} \mathbf{x}_1^{(k)} + \mathbf{H}_1^{(k,k)} \mathbf{x}_2^{(k)} + \sum_{i=1, i \neq k}^K \mathbf{H}_1^{(k,i)} \mathbf{x}^{(i)} + \mathbf{n}_1^{(k)} \quad (9a)$$

$$\mathbf{y}_2^{(k)} = \mathbf{H}_2^{(k,k)} \mathbf{x}_2^{(k)} + \mathbf{H}_2^{(k,k)} \mathbf{x}_1^{(k)} + \sum_{i=1, i \neq k}^K \mathbf{H}_2^{(k,i)} \mathbf{x}^{(i)} + \mathbf{n}_2^{(k)} \quad (9b)$$

where $\mathbf{n}_m^{(k)} \in \mathbb{C}^{M_k \times 1}$ ($m = 1, 2$) represents the additive Gaussian noise with identical elements of $\mathcal{CN}(0, \sigma^2)$ distributions.

Without loss of generality, we assume user 1 is the near user who implements the SIC and user 2 is the far user. As aforementioned, the coastal ship and the low-end maritime device could be a common case of the paired users. According to the rule of NOMA, user 1 first decodes the message

of user 2 and then removes it from the received signal, subsequently decoding its own message. Considering the inter-cluster interference, the covariance matrix of interference plus noise of user 1 in cluster k ($k = 1, \dots, K$) is given by

$$\bar{\mathbf{Z}}_1^{(k)} = \mathbf{E}_S \left[\sum_{i=1, i \neq k}^K \mathbf{H}_1^{(k,i)} \mathbf{P}^{(i)} \mathbf{H}_1^{(k,i)H} + \sigma^2 \mathbf{I}_{M_k} \right] \quad (10a)$$

$$= \left(\sum_{i=1, i \neq k}^K \sum_{n=1}^{T_i + U_i} l_{1,n}^{(k,i)} P_n^{(i)} + \sigma^2 \right) \mathbf{I}_{T_k + U_k} \quad (10b)$$

where \mathbf{E}_S is the expectation operator over small-scale fading $\mathcal{S} = \{\mathbf{S}_m^{(k,i)} | k, i = 1, \dots, K\}$, $\mathbf{P}^{(i)}$ is the power matrix of cluster i , i.e., $\mathbf{P}^{(i)} = \text{diag}\{P_1^{(i)}, \dots, P_{T_i + U_i}^{(i)}\}$ and $\mathbf{P}^{(i)} = \mathbf{P}_1^{(i)} + \mathbf{P}_2^{(i)}$. $\mathbf{P}_m^{(i)}$ ($m = 1, 2$) represents the power matrix of user m in cluster i , i.e., $\mathbf{P}_m^{(i)} = \text{diag}\{P_{m,1}^{(i)}, \dots, P_{m,T_i + U_i}^{(i)}\}$. Correspondingly, we denote $\sigma_{k,1}^2(\mathbf{P})$ as

$$\sigma_{k,1}^2(\mathbf{P}) = \sum_{i=1, i \neq k}^K \sum_{n=1}^{T_i + U_i} l_{1,n}^{(k,i)} P_n^{(i)} + \sigma^2 \quad (11)$$

and $\mathbf{P} = \{\mathbf{P}^{(i)} | i = 1, \dots, K\}$.

As for user 2, it regards user 1's signal as the background noise and directly decodes its own message. With the inter-cluster and inter-user interference, the interference plus noise of user 2 is calculated by

$$\sigma_{k,2}^2(\mathbf{P}) = \sum_{i=1, i \neq k}^K \sum_{n=1}^{T_i + U_i} l_{2,n}^{(k,i)} P_n^{(i)} + \sum_{n=1}^{T_k + U_k} l_{2,n}^{(k,k)} P_{1,n}^{(k)} + \sigma^2. \quad (12)$$

When only large-scale CSI is known at transmitters, the ergodic rate of user m ($m = 1, 2$) in cluster k ($k = 1, \dots, K$) can be expressed as

$$\bar{R}_{k,m}(\mathbf{P}) = \mathbf{E}_S \left[\log_2 \det \left(\mathbf{I}_{M_k} + \frac{\mathbf{H}_m^{(k,k)} \mathbf{P}_m^{(k)} \mathbf{H}_m^{(k,k)H}}{\sigma_{k,m}^2(\mathbf{P})} \right) \right]. \quad (13)$$

To ensure the NOMA principle is applicable, user 1 should be capable to decode the message of user 2. Strictly speaking, if the theoretical rate that user 1 receives the message of user 2, i.e., $\hat{R}_{k,1}(\mathbf{P})$ is larger than the rate of user 2, thus, user 1 is competent to implement the SIC. The rate condition is given by

$$\bar{R}_{k,2}(\mathbf{P}) \leq \hat{R}_{k,1}(\mathbf{P}), k = 1, \dots, K \quad (14)$$

where $\hat{R}_{k,1}(\mathbf{P})$ and $\hat{\sigma}_{k,1}^2(\mathbf{P})$ are as follows

$$\hat{R}_{k,1}(\mathbf{P}) = \mathbf{E}_S \left[\log_2 \det \left(\mathbf{I}_{M_k} + \frac{\mathbf{H}_1^{(k,k)} \mathbf{P}_2^{(k)} \mathbf{H}_1^{(k,k)H}}{\hat{\sigma}_{k,1}^2(\mathbf{P})} \right) \right], \quad (15)$$

$$\hat{\sigma}_{k,1}^2(\mathbf{P}) = \sum_{i=1, i \neq k}^K \sum_{n=1}^{T_i + U_i} l_{1,n}^{(k,i)} P_n^{(i)} + \sum_{n=1}^{T_k + U_k} l_{1,n}^{(k,k)} P_{1,n}^{(k)} + \sigma^2. \quad (16)$$

As we can see, the rate condition does not require user 1 dominates in all channels. Since the TBSs and UAVs are distributed in different positions, there is a complicated relationship of the decoding order and user positions. It is

an interesting problem to investigate the pairing scheme for the distributed antenna system and considerable gains can be achieved if we take both user pairing and resource allocation into account [26]. For simplicity, in this paper, we focus on the case that user 1 and user 2 are separated by a large distance so that the constraint (14) can be sufficiently guaranteed. This situation also accords with the wide sparsity of maritime IoT.

Since we assume user 1 possesses better channels, traditional opportunistic schemes tend to give more resources to user 1 to exploit more efficiency. This greatly influences the fairness of the network. So, to take care of the basic QoS requirement of user 2, i.e., r_k , we impose the following constraint

$$\bar{R}_{k,2}(\mathbf{P}) \geq r_k, \quad k = 1, \dots, K. \quad (17)$$

Furthermore, to protect satellite signals from potential impairment, the sum interference from the nearshore network is restricted by the maximum tolerable threshold of satellite receivers, i.e., \bar{P} . The constraint is expressed by

$$\sum_{k=1}^K \mathbf{E}_{\mathbf{s}'} \|\mathbf{h}'^{(j,k)} \mathbf{P}^{(k)} \mathbf{h}'^{(j,k)H}\| \leq \bar{P}, \quad j = 1, \dots, J. \quad (18)$$

where $\mathbf{s}' = \{\mathbf{s}'^{(j,k)} | j = 1, \dots, J, k = 1, \dots, K\}$. Based on the Gaussian distribution of \mathbf{s}' , the left side of (18) can be converted as follows

$$\sum_{k=1}^K \mathbf{E}_{\mathbf{s}'} \|\mathbf{h}'^{(j,k)} \mathbf{P}^{(k)} \mathbf{h}'^{(j,k)H}\| = \sum_{k=1}^K \sum_{n=1}^{T_k+U_k} l_n^{(j,k)} P_n^{(k)}. \quad (19)$$

From the practical perspective, we have the maximum affordable transmit power of both TBSs and UAVs, i.e., P_{Tmax} and P_{Umax} , and the power budget of each cluster, i.e., P_{max} , which are given by

$$P_n^{(k)} \leq P_{\text{Tmax}}, \quad n = 1, \dots, T_k, \quad (20a)$$

$$P_n^{(k)} \leq P_{\text{Umax}}, \quad n = T_k + 1, \dots, T_k + U_k, \quad (20b)$$

$$\text{tr}(\mathbf{P}^{(k)}) \leq P_{\text{max}}, \quad k = 1, \dots, K. \quad (20c)$$

Aiming at maximizing the ergodic sum rate of K clusters, i.e., $\bar{R}(\mathbf{P}) = \sum_{k=1}^K \sum_{m=1}^2 \bar{R}_{k,m}(\mathbf{P})$, the power allocation problem is formulated as

$$(\text{P1}) \max_{\mathbf{P}} \bar{R}(\mathbf{P}) \quad (21a)$$

$$s.t. \quad \bar{R}_{k,2}(\mathbf{P}) \geq r_k \quad (21b)$$

$$\mathbf{P}^{(k)} \succeq 0 \quad (21c)$$

$$\text{tr}(\mathbf{P}^{(k)}) \leq P_{\text{max}} \quad (21d)$$

$$P_n^{(k)} \leq P_{\text{Tmax}}, \quad n = 1, \dots, T_k \quad (21e)$$

$$P_n^{(k)} \leq P_{\text{Umax}}, \quad n = T_k + 1, \dots, T_k + U_k \quad (21f)$$

$$\sum_{k=1}^K \sum_{n=1}^{T_k+U_k} P_n^{(k)} l_n^{(j,k)} \leq \bar{P}, \quad j = 1, \dots, J \quad (21g)$$

$k = 1, \dots, K.$

The problem is quite complex due to the implicit expression of the ergodic rate. The tricky expectation operations should

be first removed. By leveraging the random matrix theory, $\bar{R}_{k,m}(\mathbf{P})$ ($m = 1, 2, k = 1, \dots, K$) can be approximated into a closed-form expression without the expectation operation [27]

$$\bar{R}_{k,m}(\mathbf{P}) \approx g_{k,m}(\mathbf{P}, v_{k,m}^*) \quad (22a)$$

$$g_{k,m}(\mathbf{P}, v_{k,m}^*) = \sum_{n=1}^{T_k+U_k} \log_2 \left(1 + \frac{M_k l_{m,n}^{(k,k)} P_{m,n}^{(k)}}{v_{k,m}^* \sigma_{k,m}^2(\mathbf{P})} \right) + M_k \log_2 v_{k,m}^* - M_k \log_2 e [1 - (v_{k,m}^*)^{-1}] \quad (22b)$$

where $v_{k,m}^*$ is given by the following equation

$$v_{k,m}^* = 1 + \sum_{n=1}^{T_k+U_k} \frac{l_{m,n}^{(k,k)} P_{m,n}^{(k)}}{\sigma_{k,m}^2(\mathbf{P}) + M_k l_{m,n}^{(k,k)} P_{m,n}^{(k)} (v_{k,m}^*)^{-1}}. \quad (23)$$

Then, the original problem (P1) is recast into (P2) as follows

$$(\text{P2}) \max_{\mathbf{P}} g(\mathbf{P}, \mathbf{v}^*) \quad (24a)$$

$$s.t. \quad g_{k,2}(\mathbf{P}, v_{k,2}^*) \geq r_k \quad (24b)$$

$$\mathbf{P}^{(k)} \succeq 0 \quad (24c)$$

$$\text{tr}(\mathbf{P}^{(k)}) \leq P_{\text{max}} \quad (24d)$$

$$P_n^{(k)} \leq P_{\text{Tmax}}, \quad n = 1, \dots, T_k \quad (24e)$$

$$P_n^{(k)} \leq P_{\text{Umax}}, \quad n = T_k + 1, \dots, T_k + U_k \quad (24f)$$

$$\sum_{k=1}^K \sum_{n=1}^{T_k+U_k} P_n^{(k)} l_n^{(j,k)} \leq \bar{P}, \quad j = 1, \dots, J \quad (24g)$$

$k = 1, \dots, K.$

where $g(\mathbf{P}, \mathbf{v}^*) = \sum_{k=1}^K \sum_{m=1}^2 g_{k,m}(\mathbf{P}, v_{k,m}^*)$ and $\mathbf{v}^* = \{v_{k,m}^* | m = 1, 2, k = 1, \dots, K\}$.

B. Relaxations of the Non-Linear Constraint

Although we get rid of the expectation operations in (P2), the introduced implicit parameters \mathbf{v}^* with an extra group of complex non-linear equations (23) lead to great difficulties to solve this problem. Trapped by these fixed points, the rate expressions in the non-linear QoS constraint (24b) is hard to be simplified. To tackle this challenge, we first apply one relaxation to divorce these fixed points from the rate expressions. Then, another relaxation is applied to eliminate the fixed points in the constraint. The two relaxations are derived in the following.

Theorem 1: The fixed point $v_{k,2}^*$ ($k = 1, \dots, K$) can be divorced from the rate expression $g_{k,2}(\mathbf{P}, v_{k,2}^*)$ by rewriting it into an optimization form with the condition of $M_k \geq T_k + U_k$

$$g_{k,2}(\mathbf{P}, v_{k,2}^*) = \max_{z_k \leq v_{k,2}^*} f_{k,2}(\mathbf{P}, z_k) \quad (25)$$

where $f_{k,2}(\mathbf{P}, z_k)$ ($k = 1, \dots, K$) is a monotonically increasing function with respect to z_k and it is given by

$$f_{k,2}(\mathbf{P}, z_k) = \sum_{n=1}^{T_k+U_k} \left(\log_2 \left(1 + \frac{M_k l_{2,n}^{(k,k)} P_{2,n}^{(k)}}{z_k \sigma_{k,2}^2(\mathbf{P})} \right) - \frac{\log_2(e) M_k l_{2,n}^{(k,k)} P_{2,n}^{(k)}}{z_k \sigma_{k,2}^2(\mathbf{P}) + M_k l_{2,n}^{(k,k)} P_{2,n}^{(k)}} \right) + M_k \log_2 z_k. \quad (26)$$

Proof: See Appendix A.

With the assumption that $M_k \geq T_k + U_k$, it is easy to find if $z_k \in [1, v_{k,2}^*]$, the function $f_{k,2}(\mathbf{P}, z_k)$ reaches to its maximum when $z_k = v_{k,2}^*$ and the equation $f_{k,2}(\mathbf{P}, z_k) = g_{k,2}(\mathbf{P}, v_{k,2}^*)$ holds. Based on the relaxation method, (P2) can be equivalently relaxed into (P3) as follows

$$(P3) \max_{\mathbf{P}, z_k} g(\mathbf{P}, \mathbf{v}^*) \quad (27a)$$

$$s.t. \quad f_{k,2}(\mathbf{P}, z_k) \geq r_k \quad (27b)$$

$$1 \leq z_k \leq v_{k,2}^* \quad (27c)$$

$$\mathbf{P}^{(k)} \succeq 0 \quad (27d)$$

$$\text{tr}(\mathbf{P}^{(k)}) \leq P_{\max} \quad (27e)$$

$$P_n^{(k)} \leq P_{\max}, n = 1, \dots, T_k \quad (27f)$$

$$P_n^{(k)} \leq P_{\max}, n = T_k + 1, \dots, T_k + U_k \quad (27g)$$

$$\sum_{k=1}^K \sum_{n=1}^{T_k+U_k} P_n^{(k)} l_n'^{(j,k)} \leq \bar{P}, j = 1, \dots, J \quad (27h)$$

$$k = 1, \dots, K.$$

It is clear that the fixed points $v_{k,2}^*$ ($k = 1, \dots, K$) are relaxed into z_k ($k = 1, \dots, K$) so that they are divorced from the rate expressions. But they still exist in (27c). To further simplify this problem, another relaxation is derived as follows.

$f_{k,2}(\mathbf{P}, z_k)$ ($k = 1, \dots, K$) can be reorganized as

$$f_{k,2}(\mathbf{P}, z_k) = - \sum_{n=1}^{T_k+U_k} \left(\frac{\log_2(e) M_k l_{2,n}^{(k,k)} P_{2,n}^{(k)}}{z_k \sigma_{k,2}^2(\mathbf{P}) + M_k l_{2,n}^{(k,k)} P_{2,n}^{(k)}} + \log_2 \left(1 - \frac{M_k l_{2,n}^{(k,k)} P_{2,n}^{(k)}}{z_k \sigma_{k,2}^2(\mathbf{P}) + M_k l_{2,n}^{(k,k)} P_{2,n}^{(k)}} \right) \right) + M_k \log_2 z_k \quad (28)$$

where the fraction parts just right have the same structure. Motivated by this, we use $\mathbf{t}_k^* = \{t_{k,n}^* | n = 1, \dots, T_k + U_k\}$ ($k = 1, \dots, K$) to replace these fractions and $t_{k,n}^*$ is defined by

$$t_{k,n}^* = \frac{M_k l_{2,n}^{(k,k)} P_{2,n}^{(k)}}{z_k \sigma_{k,2}^2(\mathbf{P}) + M_k l_{2,n}^{(k,k)} P_{2,n}^{(k)}}. \quad (29)$$

So, $f_{k,2}(\mathbf{P}, z_k)$ can be rewritten as $f_{k,2}(z_k, \mathbf{t}_k^*)$ as

$$f_{k,2}(z_k, \mathbf{t}_k^*) = - \sum_{n=1}^{T_k+U_k} \log_2 e(t_{k,n}^* + \ln(1 - t_{k,n}^*)) + M_k \log_2 z_k. \quad (30)$$

Obviously, $f_{k,2}(z_k, \mathbf{t}_k^*)$ is in a much simplified form compared to $f_{k,2}(\mathbf{P}, z_k)$. Based on this, we further investigate the relationship between $f_{k,2}(z_k, \mathbf{t}_k^*)$ and $g_{k,2}(\mathbf{P}, v_{k,2}^*)$ and accordingly derive a more tractable way to express $g_{k,2}(\mathbf{P}, v_{k,2}^*)$.

Theorem 2: The rate expression $g_{k,2}(\mathbf{P}, v_{k,2}^*)$ can be monotized into the maximization of $\mathcal{F}_{k,2}(z_k, \mathbf{t}_k)$

$$g_{k,2}(\mathbf{P}, v_{k,2}^*) = \max_{1 \leq z_k \leq v_{k,2}^*, 0 \leq \mathbf{t}_k \leq \mathbf{t}_k^*} \mathcal{F}_{k,2}(z_k, \mathbf{t}_k) \quad (31)$$

where $\mathcal{F}_{k,2}(z_k, \mathbf{t}_k)$ ($k = 1, \dots, K$) is monotonically increasing with respect to z_k and \mathbf{t}_k and it is defined by

$$\mathcal{F}_{k,2}(z_k, \mathbf{t}_k) = - \sum_{n=1}^{T_k+U_k} \log_2 e(t_{k,n} + \ln(1 - t_{k,n})) + M_k \log_2 z_k. \quad (32)$$

The constraint $z_k \leq v_{k,2}^*$ is equivalent to the following two inequalities

$$z_k \leq v_{k,2}^* \Leftrightarrow \begin{cases} (z_k)^{-1} + \frac{1}{M_k} \sum_{n=1}^{T_k+U_k} t_{k,n} \geq 1, \\ t_{k,n} \leq t_{k,n}^*, n = 1, \dots, T_k + U_k. \end{cases} \quad (33)$$

Proof: See Appendix B.

It can be seen that by introducing the slack variables \mathbf{t}_k ($k = 1, \dots, K$), $g_{k,2}(\mathbf{P}, v_{k,2}^*)$ is further recast into the optimization of $\mathcal{F}_{k,2}(z_k, \mathbf{t}_k)$ with two much simplified constraints corresponding to $z_k \leq v_{k,2}^*$. Again, by leveraging the relaxation method, (P3) can be recast into (P4) as follows

$$(P4) \max_{\mathbf{P}, z_k, \mathbf{t}_k} g(\mathbf{P}, \mathbf{v}^*) \quad (34a)$$

$$s.t. \quad \mathcal{F}_{k,2}(z_k, \mathbf{t}_k) \geq r_k \quad (34b)$$

$$(z_k)^{-1} + \frac{1}{M_k} \sum_{n=1}^{T_k+U_k} t_{k,n} \geq 1 \quad (34c)$$

$$t_{k,n} \leq t_{k,n}^* \quad (34d)$$

$$t_{k,n} \geq 0 \quad (34e)$$

$$z_k \geq 1 \quad (34f)$$

$$\mathbf{P}^{(k)} \succeq 0 \quad (34g)$$

$$\text{tr}(\mathbf{P}^{(k)}) \leq P_{\max} \quad (34h)$$

$$P_n^{(k)} \leq P_{\max}, n = 1, \dots, T_k \quad (34i)$$

$$P_n^{(k)} \leq P_{\max}, n = T_k + 1, \dots, T_k + U_k \quad (34j)$$

$$\sum_{k=1}^K \sum_{n=1}^{T_k+U_k} P_n^{(k)} l_n'^{(j,k)} \leq \bar{P}, j = 1, \dots, J \quad (34k)$$

$$n = 1, \dots, T_k + U_k \text{ and } k = 1, \dots, K.$$

Up to now, the QoS constraint (24b) in (P2) has been relaxed into five constraints (34b), (34c), (34d), (34e) and (34f) in (P4) and the fixed points $v_{k,2}^*$ ($k = 1, \dots, K$) therein have been totally removed. We want to note that if the constraint (24b) in (P2) is tight, the optimal solution of (P4) is obtained if and only if $\mathcal{F}_{k,2}(z_k, \mathbf{t}_k)$ is maximized, which in terms indicates that the equations hold in (34b), (34c) and (34d), and $\mathcal{F}_{k,2}(z_k, \mathbf{t}_k) = g_{k,2}(\mathbf{P}, v_{k,2}^*)$. So, it is easy to find that the above two relaxations do not change the optimal solution and (P4) is equivalent to (P2).

C. Equivalent Max-Min Problem and Iterative Solution

As we can see, problem (P4) is much simplified, but the troublesome fixed points are still in the objective function. By analyzing the monotonicity of $g_{k,m}(\mathbf{P}, v_{k,m})$ ($m = 1, 2, k = 1, \dots, K$), it is proved that $g_{k,m}(\mathbf{P}, v_{k,m})$ is monotonically decreasing with $v_{k,m}$ in $[1, v_{k,m}^*]$ and monotonically increasing in $[v_{k,m}^*, +\infty)$ [27]. As $v_{k,m}^*$ is the extreme point of $g_{k,m}(\mathbf{P}, v_{k,m})$, it can be calculated by the minimum operation as

$$g_{k,m}(\mathbf{P}, v_{k,m}^*) = \min_{1 \leq v_{k,m}} g_{k,m}(\mathbf{P}, v_{k,m}) \quad (35)$$

where $g_{k,m}(\mathbf{P}, v_{k,m})$ is quasi-convex with respect to $v_{k,m}$. In order to transform it into a convex expression, define $e^{w_{k,m}} =$

$v_{k,m}$ ($m = 1, 2, k = 1, \dots, K$) and $g_{k,m}(\mathbf{P}, v_{k,m})$ ($k = 1, \dots, K$) can be recast into $\mathcal{G}_{k,m}(\mathbf{P}, w_{k,m})$ as follows

$$\mathcal{G}_{k,m}(\mathbf{P}, w_{k,m}) = \sum_{n=1}^{T_k+U_k} \log_2 \left(1 + \frac{M_k l_{m,n}^{(k,k)} P_{m,n}^{(k)}}{e^{w_{k,m}} \sigma_{k,m}^2(\mathbf{P})} \right) + M_k \log_2 e [w_{k,m} + e^{-w_{k,m}} - 1] \quad (36)$$

which is convex with respect to $w_{k,m}$. Replaced by the minimal operations, the fixed points are totally eliminated and the problem is transformed into a max-min problem as below

$$(P5) \max_{\mathbf{P}, z_k, \mathbf{t}_k} \min_{\mathbf{w}} \mathcal{G}(\mathbf{P}, \mathbf{w}) \quad (37a)$$

$$s.t. \mathcal{F}_{k,2}(z_k, \mathbf{t}_k) \geq r_k \quad (37b)$$

$$(z_k)^{-1} + \frac{1}{M_k} \sum_{n=1}^{T_k+U_k} t_{k,n} \geq 1 \quad (37c)$$

$$t_{k,n} \leq t_{k,n}^* \quad (37d)$$

$$t_{k,n} \geq 0 \quad (37e)$$

$$z_k \geq 1 \quad (37f)$$

$$w_{k,m} \geq 0 \quad (37g)$$

$$\mathbf{P}^{(k)} \succeq 0 \quad (37h)$$

$$\text{tr}(\mathbf{P}^{(k)}) \leq P_{\max} \quad (37i)$$

$$P_n^{(k)} \leq P_{\max}, n = 1, \dots, T_k \quad (37j)$$

$$P_n^{(k)} \leq P_{\max}, n = T_k + 1, \dots, T_k + U_k \quad (37k)$$

$$\sum_{k=1}^K \sum_{n=1}^{T_k+U_k} P_n^{(k)} l_n'^{(j,k)} \leq \bar{P}, j = 1, \dots, J \quad (37l)$$

$$m = 1, 2, n = 1, \dots, T_k + U_k, k = 1, \dots, K,$$

where $\mathcal{G}(\mathbf{P}, \mathbf{w}) = \sum_{k=1}^K \sum_{m=1}^2 \mathcal{G}_{k,m}(\mathbf{P}, w_{k,m})$ and $\mathbf{w} = \{w_{k,m} | m = 1, 2, k = 1, \dots, K\}$. In order to decouple different optimization variables in (37d), we apply the logarithmic operation on its both sides and reorganize it into the following expression

$$\ln(M_k P_{2,n}^{(k)} l_{2,n}^{(k,k)}) + \ln(1 - t_{k,n}) \geq \ln(z_k) + \ln(t_{k,n}) + \ln(\sigma_{k,2}^2(\mathbf{P})). \quad (38)$$

As for the objective function, $\mathcal{G}_{k,m}(\mathbf{P}, w_{k,m})$ can be decomposed into two parts as

$$\mathcal{G}_{k,m}(\mathbf{P}, w_{k,m}) = \mathcal{G}_{k,m,1}(\mathbf{P}, w_{k,m}) - \mathcal{G}_{k,m,2}(\mathbf{P}) \quad (39)$$

where

$$\mathcal{G}_{k,m,1}(\mathbf{P}, w_{k,m}) = \sum_{n=1}^{T_k+U_k} \log_2 \left(\sigma_{k,m}^2(\mathbf{P}) + \frac{M_k l_{m,n}^{(k,k)} P_{m,n}^{(k)}}{e^{w_{k,m}}} \right) + M_k \log_2 e [w_{k,m} + e^{-w_{k,m}} - 1] \quad (40a)$$

$$\mathcal{G}_{k,m,2}(\mathbf{P}) = (T_k + U_k) \log_2 \sigma_{k,m}^2(\mathbf{P}) \quad (40b)$$

are both concave with respect to \mathbf{P} . Although the subtraction of two concave expressions may not maintain the concave property, the Taylor expansion can be applied to obtain the

concave function at the given point. Thus, based on the method of successive convex approximation, a corresponding iterative solution is further proposed.

At the beginning, we give the initial point \mathbf{P}^0 so that z_k^0 as well as \mathbf{t}_k^0 ($k = 1, \dots, K$) can be obtained according to (23) and (29). Then based on (38) and (39), we can find that all the separate terms in (P5) are either concave or convex. In order to transform our problem into a standard convex problem, we can linearize those terms violating the convex optimization rule. They are $\mathcal{G}_{k,m,2}(\mathbf{P})$ in (37a), $\log_2(1 - t_{k,n})$ in (37b), $(z_k)^{-1}$ in (37c), and $\ln(z_k) + \ln(t_{k,n}) + \ln(\sigma_{k,2}^2(\mathbf{P}))$ in (38).

In each iteration s ($s = 1, 2, \dots$), given points \mathbf{P}^{s-1} , z_k^{s-1} and \mathbf{t}_k^{s-1} ($k = 1, \dots, K$), the convex subproblem can be formulated as

$$(P6) \max_{\mathbf{P}, z_k, \mathbf{t}_k} \min_{\mathbf{w}} \mathcal{G}(\mathbf{P}, \mathbf{w} | \mathbf{P}^{s-1}) \quad (41a)$$

$$s.t. \mathcal{F}_{k,2}(z_k, \mathbf{t}_k | \mathbf{t}_k^{s-1}) \geq r_k \quad (41b)$$

$$-\frac{z_k}{(z_k^{s-1})^2} + \frac{2}{z_k^{s-1}} + \frac{1}{M_k} \sum_{n=1}^{T_k+U_k} t_{k,n} \geq 1 \quad (41c)$$

$$\ln(M_k P_{2,n}^{(k)} l_{2,n}^{(k,k)}) + \ln(1 - t_{k,n}) \geq \quad (41d)$$

$$\ln(z_k | z_k^{s-1}) + \ln(t_{k,n} | t_{k,n}^{s-1}) + \ln(\sigma_{k,2}^2(\mathbf{P} | \mathbf{P}^{s-1}))$$

$$z_k \geq 1 \quad (41e)$$

$$t_{k,n} \geq 0 \quad (41f)$$

$$w_{k,m} \geq 0 \quad (41g)$$

$$\mathbf{P}^{(k)} \succeq 0 \quad (41h)$$

$$\text{tr}(\mathbf{P}^{(k)}) \leq P_{\max} \quad (41i)$$

$$P_n^{(k)} \leq P_{\max}, n = 1, \dots, T_k \quad (41j)$$

$$P_n^{(k)} \leq P_{\max}, n = T_k + 1, \dots, T_k + U_k \quad (41k)$$

$$\sum_{k=1}^K \sum_{n=1}^{T_k+U_k} P_n^{(k)} l_n'^{(j,k)} \leq \bar{P}, j = 1, \dots, J \quad (41l)$$

$$m = 1, 2, n = 1, \dots, T_k + U_k, k = 1, \dots, K.$$

In each iteration, the obtained optimal solution $(\mathbf{P}^s, \mathbf{w}^s)$ is the saddle point of $\mathcal{G}(\mathbf{P}, \mathbf{w} | \mathbf{P}^{s-1})$. The expressions $\mathcal{G}(\mathbf{P}, \mathbf{w} | \mathbf{P}^{s-1})$, $\mathcal{F}_{k,2}(z_k, \mathbf{t}_k | \mathbf{t}_k^{s-1})$ and $\ln(z_k | z_k^{s-1}) + \ln(t_{k,n} | t_{k,n}^{s-1}) + \ln(\sigma_{k,2}^2(\mathbf{P} | \mathbf{P}^{s-1}))$ are the first-order Taylor expansions of $\mathcal{G}(\mathbf{P}, \mathbf{w})$, $\mathcal{F}_{k,2}(z_k, \mathbf{t}_k)$ and $\ln(z_k) + \ln(t_{k,n}) + \ln(\sigma_{k,2}^2(\mathbf{P}))$. Their expressions as well as $\sigma_{k,1}^2(\mathbf{P} | \mathbf{P}^{s-1})$, $\sigma_{k,2}^2(\mathbf{P} | \mathbf{P}^{s-1})$ are shown at the top of the next page. The details of the algorithm are summarized in Algorithm 1 and the convergence proof is given in Appendix C.

IV. SIMULATION RESULTS AND DISCUSSIONS

In this section, we evaluate the proposed scheme through simulation. Without loss of generality, we assume there are three nearshore clusters, i.e., $K = 3$, consisting of $T_1 = T_3 = 2$, $T_2 = 1$ TBSs, $U_1 = U_3 = 1$, $U_2 = 2$ UAVs. In each cluster, there are two NOMA users that are within 100km from the coastline. Both TBSs and UAVs are equipped with a single omnidirectional antenna and the NOMA users have three antennas, i.e., $g_t = 30$ dBi, $g_u = 10$ dBi, $M_1 = M_2 = M_3 = 3$. The minimum rate requirement of

$$\sigma_{k,1}^2(\mathbf{P}|\mathbf{P}^{s-1}) = \sum_{i=1, i \neq k}^K \sum_{n=1}^{T_i+U_i} l_{1,n}^{(k,i)} (P_n^{(i)} - (P_n^{(i)})^{s-1}) + \sigma^2, \quad (42a)$$

$$\sigma_{k,2}^2(\mathbf{P}|\mathbf{P}^{s-1}) = \sum_{i=1, i \neq k}^K \sum_{n=1}^{T_i+U_i} l_{2,n}^{(k,i)} (P_n^{(i)} - (P_n^{(i)})^{s-1}) + \sum_{n=1}^{T_k+U_k} l_{2,n}^{(k,k)} (P_{1,n}^{(k)} - (P_{1,n}^{(k)})^{s-1}) + \sigma^2. \quad (42b)$$

$$\begin{aligned} \mathcal{G}_{k,m}(\mathbf{P}, w_{k,m}|\mathbf{P}^{s-1}) &= \mathcal{G}_{k,m,1}(\mathbf{P}, w_{k,m}) - \mathcal{G}_{k,m,2}(\mathbf{P}|\mathbf{P}^{s-1}) \\ &= \mathcal{G}_{k,m,1}(\mathbf{P}, w_{k,m}) - \mathcal{G}_{k,m,2}(\mathbf{P}^{s-1}) - (T_k + U_k) \log_2 e \frac{\sigma_{k,m}^2(\mathbf{P}|\mathbf{P}^{s-1})}{\sigma_{k,m}^2(\mathbf{P}^{s-1})}, \end{aligned} \quad (43a)$$

$$\mathcal{G}(\mathbf{P}, \mathbf{w}|\mathbf{P}^{s-1}) = \sum_{k=1}^K \sum_{m=1}^2 \mathcal{G}_{k,m}(\mathbf{P}, w_{k,m}|\mathbf{P}^{s-1}). \quad (43b)$$

$$\mathcal{F}_{k,2}(z_k, \mathbf{t}_k|\mathbf{t}_k^{s-1}) = M_k \log_2 z_k + \sum_{n=1}^{T_k+U_k} \left(\log_2 e \frac{(t_{k,n} - 1)t_{k,n}^{s-1}}{1 - t_{k,n}^{s-1}} - \log_2(1 - t_{k,n}^{s-1}) \right). \quad (44)$$

$$\ln(z_k|z_k^{s-1}) + \ln(t_{k,n}|t_{k,n}^{s-1}) + \ln(\sigma_{k,2}^2(\mathbf{P}|\mathbf{P}^{s-1})) = \frac{z_k}{z_k^{s-1}} + \frac{t_{k,n}}{t_{k,n}^{s-1}} + \frac{\sigma_{k,2}^2(\mathbf{P}|\mathbf{P}^{s-1})}{\sigma_{k,2}^2(\mathbf{P}^{s-1})} + \ln(z_k^{s-1} t_{k,n}^{s-1} \sigma_{k,2}^2(\mathbf{P}^{s-1})) - 2. \quad (45)$$

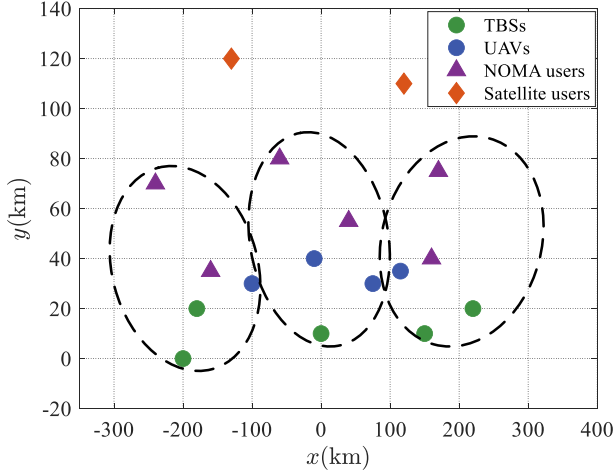


Fig. 2. Illustration of the network topology for simulations.

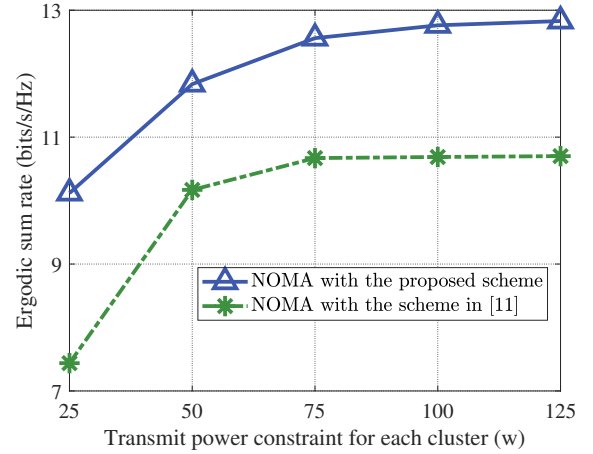


Fig. 3. The ergodic sum rate with different power allocation schemes under the NOMA regime.

user 2 is 0.5 bits/s/Hz, i.e., $r_k = 0.5$ bits/s/Hz ($k = 1, \dots, K$). Out of the coverage of the clusters, two satellite users are also considered in our setting, i.e., $J = 2$. The maximum tolerable interference of satellite users is -100 dBm, i.e., $\bar{P} = -100$ dBm, the maximum transmit power of TBSs is 40w, the maximum transmit power of UAVs is 30w, i.e., $P_{\text{Tmax}} = 40$ w, $P_{\text{Umax}} = 30$ w and the maximum transmit power for each cluster changes from 25w to 125w. The height of UAVs, TBSs and user terminals are assumed to be $h_u = 800$ m, $h_t = 200$ m and $h_r = 5$ m, respectively. The constants are given by $c = 3 \times 10^8$ m/s, $\sigma^2 = -107$ dBm, $f_c = 2$ GHz, $a = 5.0188$, $b = 0.3511$, $c = 3 \times 10^8$ m/s, $\eta_{\text{LOS}} = 0.1$, $\eta_{\text{NLOS}} = 21$ and $C = 1$.

To justify the effectiveness of our scheme, we choose a topology where near and far users are obviously separated so

that the assumption in (14) can be guaranteed. The specific distribution is shown in Fig. 2 where the positive direction of y points to the sea.

Firstly, we evaluate the proposed scheme and compare it with the scheme in [11]. As we can see from Fig. 3, the proposed scheme achieves much higher rate than that of [11]. We can also find that when the maximum transmit power exceeds 75w, increasing power cannot increase the sum rate under the scheme in [11]. This means the system is saturated due to the complex interference. For the proposed scheme, the saturate point does not yet occur in this figure. It can be explained that, based on the large-scale CSI, the system could flexibly allocate power to achieve good balance between useful signals and harmful inter-cluster interference.

Secondly, we compare the proposed scheme based on

Algorithm 1 Iterative power allocation algorithm.

Input: $P_{\max}, \bar{P}, P_{T\max}, P_{U\max}, r_k$ ($k = 1, \dots, K$)

- 1: **Initialization:** set $\epsilon = 1 \times 10^{-3}$, $(P^{(k)})^0 = P_{\max}$,
 $(P_n^{(k)})^0 = \frac{(P^{(k)})^0}{T_k + U_k}$, $n = 1, \dots, T_k + U_k$ and $k = 1, \dots, K$.
- 2: **for** $j = 1 \sim J$ **do**
- 3: **while** $(\sum_{k=1}^K \sum_{n=1}^{T_k+U_k} l_n^{(j,k)} (P_n^{(k)})^0 > \bar{P})$ **do**
- 4: $(P^{(k)})^0 = (1 - \epsilon)(P^{(k)})^0$;
- 5: $(P_n^{(k)})^0 = \frac{(P^{(k)})^0}{T_k + U_k}$, $n = 1, \dots, T_k + U_k$, $k = 1, \dots, K$;
- 6: **end while**
- 7: **end for**
- 8: **for** $k = 1 \sim K$ **do**
- 9: **for** $n = 1 \sim T_k$ **do**
- 10: **while** $((P_n^{(k)})^0 > P_{T\max})$ **do**
- 11: $(P_n^{(k)})^0 = P_{T\max}$;
- 12: **end while**
- 13: **end for**
- 14: **for** $n = T_k + 1 \sim T_k + U_k$ **do**
- 15: **while** $((P_n^{(k)})^0 > P_{U\max})$ **do**
- 16: $(P_n^{(k)})^0 = P_{U\max}$;
- 17: **end while**
- 18: **end for**
- 19: **end for**
- 20: $(P_{m,n}^{(k)})^0 = \frac{(P_n^{(k)})^0}{2}$, $m = 1, 2$, $n = 1, \dots, T_k + U_k$, and $k = 1, \dots, K$,
- 21: Calculate z_k^0 , \mathbf{t}_k^0 , $k = 1, \dots, K$ based on (23) and (29).
- 22: **Iterations:** $s = 1, 2, \dots$,
- 23: **repeat**
- 24: Update \mathbf{P}^s , \mathbf{t}_k^s and z_k^s , $k = 1, \dots, K$ by solving (P6);
- 25: **until** $\frac{\sum_{k=1}^K \sum_{m=1}^2 |\mathcal{G}_{k,m}(\mathbf{P}^s, w_{k,m}^s) - \mathcal{G}_{k,m}(\mathbf{P}^{s-1}, w_{k,m}^{s-1})|}{\sum_{k=1}^K \sum_{m=1}^2 \mathcal{G}_{k,m}(\mathbf{P}^{s-1}, w_{k,m}^{s-1})} \leq \epsilon$.

Output: \mathbf{P}^s .

NOMA with the schemes in [27] and [28] as well as the equal power allocation scheme based on OMA. Without loss of generality, the allocation coefficient of two users is set to be $\frac{1}{2}$ ¹. As shown in Fig. 4, it is obvious that the proposed scheme based on NOMA outperforms remarkably than the other three schemes based on OMA. These gains are achieved at the cost of more complex receivers. The inter-user interference is reduced by SIC. In addition, since NOMA separates users in the power domain, it provides additional flexibility to assign resources between paired users. But for OMA, it is hard to achieve the flexible time or frequency partition so that the resource efficiency is not fully exploited. Therefore, based on the SIC reception and effective resource allocation, NOMA is more capable to provide agile services for different users. In addition, one can also find that the scheme proposed in [27] performs better than the other two schemes of OMA. It can be explained by the fact that in [27], the interference is effectively controlled based on the large-scale CSI. This further shows that the positions are critical factors that can be utilized to

¹Since the scheme proposed in [27] and [28] did not consider the minimum user rate constraint, we set $r_k = 0$ bits/s/Hz ($k = 1, \dots, K$) in this simulation for comparisons.

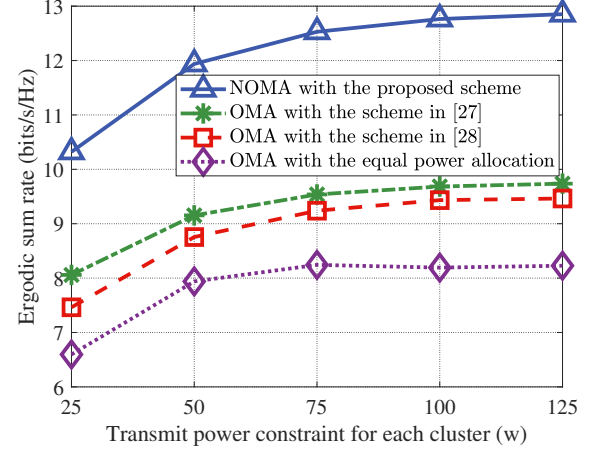


Fig. 4. The ergodic sum rate with different power allocation schemes, under both NOMA and OMA regimes.

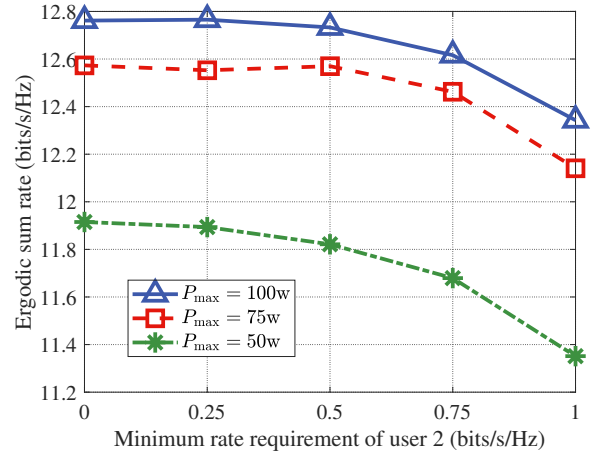


Fig. 5. The ergodic sum rate with different transmit power constraints, varying with the minimum rate requirement of user 2.

mitigate the interference especially for irregular settings.

Next, we evaluate the impact of different rate requirements of user 2. As we can see from Fig. 5, the system experiences very small performance degradation as the rate requirement increases, only less than 6% in our setting. It shows that NOMA could greatly support the wide sparsity of the maritime IoT by satisfying the basic QoS requirement of far users without sacrificing much system efficiency to give high-rate coverage for near users.

The impact of inter-segment interference is shown in Fig. 6. It can be seen that at beginning the sum rate increases with the interference constraint. This means the inter-segment interference is the bottleneck and the nearshore network has to control its power to ensure the normal operations of satellite receivers. But when the interference constraint is relaxed more than -100 dBm, the sum rate maintains unchanged. In this situation, the inter-segment interference is no longer the constraining factor, and the nearshore network and marine satellites can coexist.

Fig. 7 shows the superiority of UAVs for the coverage

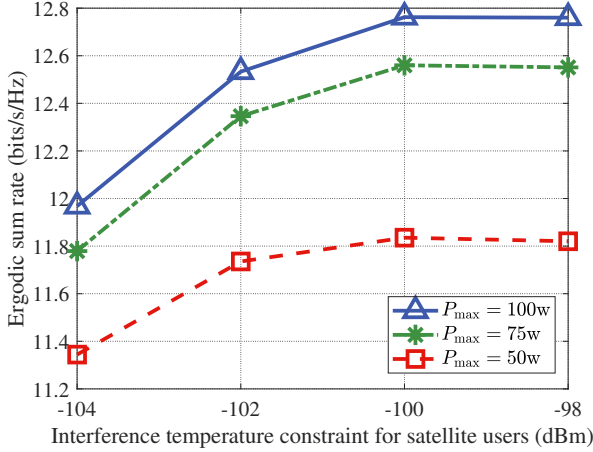


Fig. 6. The ergodic sum rate with different transmit power constraints, varying with the interference constraint of satellite users.

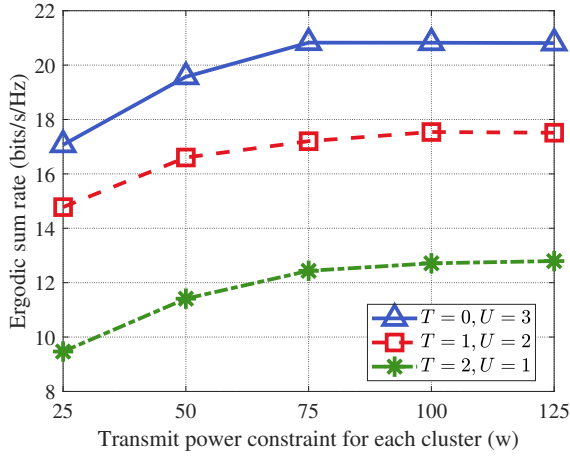


Fig. 7. The ergodic sum rate with different configurations of TBSs and UAVs.

enhancement. Different from the above settings, in this simulation, we keep the topology unchanged and replace the original TBSs with UAVs or vice versa. We set $T_1 = T_2 = T_3 = T$, $U_1 = U_2 = U_3 = U$. Obviously, UAVs bring considerable system gains compared with TBSs, with more than 50% rate improvement of one more UAV and one less TBS in our setting. Besides, we want to note that the case with only TBSs is not presented for the fact that only TBSs cannot support the basic need of user 2. This indicates that with the assistance of UAVs, the coverage scope of TBSs is enlarged. In addition, based on the height advantages, the LOS links between users and UAVs are always available. The high-quality connections can be provided by UAVs to enhance the coverage ability of the nearshore network.

Finally, the convergence of the proposed scheme is shown in Fig. 8. We randomly generate 100 different typologies with $P_{\max} = 50\text{w}$. In most cases, the proposed iterative algorithm only takes less than 10 times to converge, which shows great potentials to achieve timely resource allocation in reality.

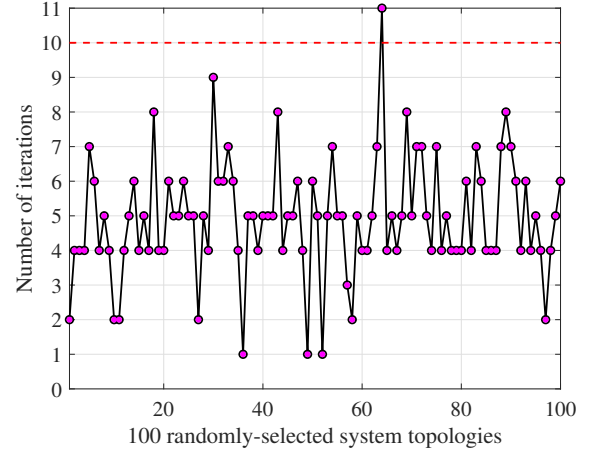


Fig. 8. Convergence performance of the proposed iterative algorithm.

V. CONCLUSIONS

In this paper, we have investigated a NOMA-based hybrid satellite-UAV-terrestrial network on the sea. Particularly, we have utilized the tethered UAVs to coordinate with TBSs. They form virtual clusters and serve users in a user-centric manner. To accommodate the wide sparsity of maritime IoT, the NOMA technique has been applied to agilely serve different users. The spectrum sharing has been considered between nearshore clusters and the marine satellites. We have proposed a joint power allocation scheme to tackle the challenging interference among different users, different clusters and different network segments. Based on large-scale CSI only, the ergodic sum rate has been maximized at a low cost. To tackle the non-convex problem, we have proposed two relaxation methods to simplify the non-linear constraint and utilized an iterative way to find the solution by solving a series of optimization-friendly max-min subproblems. Simulation results have shown the potential of NOMA-based hybrid satellite-UAV-terrestrial networks for maritime coverage enhancement.

REFERENCES

- [1] T. Wei, W. Feng, N. Ge, and J. Lu, "Environment-aware coverage optimization for space-ground integrated maritime communications," *IEEE Access*, vol. 8, pp. 89205-89214, 2020.
- [2] M. M. Wang, J. Zhang, and X. You, "Machine-type communication for maritime Internet of Things: A design," *IEEE Commun. Surveys & Tuts.*, vol. 22, no. 4, pp. 2550-2585, 4th Quart. 2020.
- [3] T. Wei, W. Feng, Y. Chen, C.-X. Wang, N. Ge, and J. Lu, "Hybrid satellite-terrestrial communication networks for the maritime Internet of Things: Key technologies, opportunities, and challenges," *IEEE Internet Things J.*, Early Access, doi: 10.1109/IIOT.2021.3056091.
- [4] X. Li, W. Feng, J. Wang, Y. Chen, N. Ge, and C.-X. Wang, "Enabling 5G on the ocean: A hybrid satellite-UAV-terrestrial network solution," *IEEE Wireless Commun.*, vol. 27, no. 6, pp. 116-121, Dec. 2020.
- [5] M. Mozaffari, W. Saad, M. Bennis, Y. Nam, and M. Debbah, "A tutorial on UAVs for wireless networks: Applications, challenges, and open problems," *IEEE Commun. Surveys & Tuts.*, vol. 21, no. 3, pp. 2334-2360, 3th Quart., 2019.
- [6] Y. Zeng, Q. Wu, and R. Zhang, "Accessing from the sky: A tutorial on UAV communications for 5G and beyond," in *Proc. IEEE*, vol. 107, no. 12, pp. 2327-2375, Dec. 2019.
- [7] Y. Li, L. Su, T. Wei, Z. Zhou, and N. Ge, "Location-aware dynamic beam scheduling for maritime communication systems," in *Proc. 2018 10th Int. Conf. Commun., Circuits and Sys. (ICCCAS)*, Chengdu, China, 2018, pp. 265-268.

- [8] M. Xu, F. Ji, M. Wen, and W. Duan, "Novel receiver design for the cooperative relaying system with non-orthogonal multiple access," *IEEE Commun. Lett.*, vol. 20, no. 8, pp. 1679-1682, Aug. 2016.
- [9] B. Zheng, M. Wen, C.-X. Wang, X. Wang, F. Chen, J. Tang, and F. Ji, "Secure NOMA based two-way relay networks using artificial noise and full duplex," *IEEE J. Sel. Areas Commun.*, vol. 36, no. 7, pp. 1426-1440, Jul. 2018.
- [10] D. Wan, M. Wen, F. Ji, H. Yu, and F. Chen, "Non-orthogonal multiple access for cooperative communications: Challenges, opportunities, and trends," *IEEE Wireless Commun.*, vol. 25, no. 2, pp. 109-117, Apr. 2018.
- [11] Q. Sun, S. Han, C. I, and Z. Pan, "On the ergodic capacity of MIMO NOMA systems," *IEEE Commun. Lett.*, vol. 4, no. 4, pp. 405-408, Aug. 2015.
- [12] Z. Ding, F. Adachi, and H. V. Poor, "The application of MIMO to non-orthogonal multiple access," *IEEE Trans. Wireless Commun.*, vol. 15, no. 1, pp. 537-552, Jan. 2016.
- [13] X. Li, W. Feng, Y. Chen, C.-X. Wang, and N. Ge, "Maritime coverage enhancement using UAVs coordinated with hybrid satellite-terrestrial networks," *IEEE Trans. Commun.*, vol. 68, no. 4, pp. 2355-2369, Apr. 2020.
- [14] Y. Wang, X. Fang, W. Feng, Y. Chen, N. Ge, and Z. Lu, "On-demand coverage for maritime hybrid satellite-UAV-terrestrial networks," in *Proc. 2020 Int. Conf. Wireless Commun. Signal Process. (WCSP)*, Nanjing, China, 2020, pp. 483-488.
- [15] J. Zhang, F. Liang, B. Li, Z. Yang, Y. Wu, and H. Zhu, "Placement optimization of caching UAV-assisted mobile relay maritime communication" *China Commun.*, vol. 17, no. 8, pp. 209-219, Aug. 2020.
- [16] A. Xiao, N. Ge, L. Yin, and C. Jiang, "A voyage-based cooperative resource allocation scheme in maritime broadband access network," in *Proc. 2017 IEEE 86th Veh. Tech. Conf. (VTC-Fall)*, Toronto, ON, Canada, 2017.
- [17] M. Hua, Y. Wang, M. Lin, C. Li, Y. Huang, and L. Yang, "Joint CoMP transmission for UAV-aided cognitive satellite terrestrial networks," *IEEE Access*, vol. 7, pp. 14959-14968, 2019.
- [18] N. Zhao, X. Pang, Z. Li, Y. Chen, F. Li, Z. Ding, and M.-S. Alouini, "Joint trajectory and precoding optimization for UAV-assisted NOMA networks," *IEEE Trans. Commun.*, vol. 67, no. 5, pp. 3723-3735, May 2019.
- [19] X. Pang, Z. Li, X. Chen, Y. Cao, N. Zhao, Y. Chen, and Z. Ding, "UAV-aided NOMA networks with optimization of trajectory and precoding," in *Proc. 2018 10th Intern. Conf. Wireless Commun. Signal Process. (WCSP)*, Hangzhou, China, 2018, pp. 1-6.
- [20] C. Liu, W. Feng, Y. Chen, C.-X. Wang, and N. Ge, "Cell-free satellite-UAV networks for 6G wide-area Internet of Things," *IEEE J. Sel. Areas Commun.*, Early Access, doi:10.1109/JSAC.2020.3018837.
- [21] Z. Lin, M. Lin, J. Wang, T. de Cola, and J. Wang, "Joint beamforming and power allocation for satellite-terrestrial integrated networks with non-orthogonal multiple access," *IEEE J. Sel. Topics Signal Process.*, vol. 13, no. 3, pp. 657-670, Jun. 2019.
- [22] L. Wang, Y. Wu, H. Zhang, S. Choi, and V. C. M. Leung, "Resource allocation for NOMA based space-terrestrial satellite networks," *IEEE Trans. Wireless Commun.*, vol. 20, no. 2, pp. 1065-1075, Feb. 2021.
- [23] S. Jo and W. Shim, "LTE-maritime: High-speed maritime wireless communication based on LTE technology," *IEEE Access*, vol. 7, pp. 53172-53181, 2019.
- [24] W. Feng, J. Wang, Y. Chen, X. Wang, N. Ge, and J. Lu, "UAV-aided MIMO communications for 5G Internet of Things," *IEEE Internet Things J.*, vol. 6, no. 2, pp. 1731-1740, Apr. 2019.
- [25] P. Wang, W. Zhang, J. Yin, L. Li, H. Xie, and S. Ma, "AIS data-based for statistics and analysis of maritime traffic dangerous features: a case study of San Diego coastal water," in *Proc. 2020 Chinese Control And Decision Conference (CCDC)*, Hefei, China, 2020, pp. 3671-3676.
- [26] Z. Ding, P. Fan, and H. V. Poor, "Impact of user pairing on 5G nonorthogonal multiple-access downlink transmissions," *IEEE Trans. Veh. Tech.*, vol. 65, no. 8, pp. 6010-6023, Aug. 2016.
- [27] W. Feng, Y. Wang, N. Ge, J. Lu, and J. Zhang, "Virtual MIMO in multi-cell distributed antenna systems: Coordinated transmissions with large-scale CSIT," *IEEE J. Sel. Areas Commun.*, vol. 31, no. 10, pp. 2067-2081, Oct. 2013.
- [28] W. Choi and J. G. Andrews, "Downlink performance and capacity of distributed antenna systems in a multicell environment," *IEEE Trans. Wireless Commun.*, vol. 6, no. 1, pp. 69-73, Jan. 2007.

APPENDIX A PROOF OF THEOREM 1

Through observations, the fixed-point equation (23) can be rewritten as

$$1 - (v_{k,m}^*)^{-1} = \sum_{n=1}^{T_k+U_k} \frac{l_{m,n}^{(k,k)} P_{m,n}^{(k)}}{v_{k,m}^* \sigma_{k,m}^2(\mathbf{P}) + M_k l_{m,n}^{(k,k)} P_{m,n}^{(k)}}. \quad (46)$$

Based on this transformation, the term $1 - (v_{k,2}^*)^{-1}$ in $g_{k,2}(\mathbf{P}, v_{k,2}^*)$ (defined in (37a)) of (24b) can be replaced by the right side of (46) taking $m = 2$. Consequently, a new function $f_{k,2}(\mathbf{P}, z_k)$ ($k = 1, \dots, K$) can be formed as follows

$$f_{k,2}(\mathbf{P}, z_k) = \sum_{n=1}^{T_k+U_k} \left(\log_2 \left(1 + \frac{M_k l_{2,n}^{(k,k)} P_{2,n}^{(k)}}{z_k \sigma_{k,2}^2(\mathbf{P})} \right) - \frac{\log_2(e) M_k l_{2,n}^{(k,k)} P_{2,n}^{(k)}}{z_k \sigma_{k,2}^2(\mathbf{P}) + M_k l_{2,n}^{(k,k)} P_{2,n}^{(k)}} \right) + M_k \log_2 z_k. \quad (47)$$

where z_k ($k = 1, \dots, K$) is the introduced variable corresponding to $v_{2,k}$ ($k = 1, \dots, K$) and we have

$$g_{k,2}(\mathbf{P}, v_{2,k}^*) = f_{k,2}(\mathbf{P}, v_{2,k}^*) \quad (48)$$

Next, we proof the monotonicity of $f_{k,2}(\mathbf{P}, z_k)$ with respect to z_k . We calculate the partial derivative of $f_{k,2}(\mathbf{P}, z_k)$ as

$$\begin{aligned} \frac{\partial f_{k,2}(\mathbf{P}, z_k)}{\partial z_k} &= \frac{\log_2 e}{z_k} \left[M_k - \sum_{n=1}^{T_k+U_k} \left(\frac{M_k l_{2,n}^{(k,k)} P_{2,n}^{(k)}}{z_k \sigma_{k,2}^2(\mathbf{P}) + M_k l_{2,n}^{(k,k)} P_{2,n}^{(k)}} \right)^2 \right] \\ &\geq \frac{\log_2 e}{z_k} [M_k - (T_k + U_k)]. \end{aligned} \quad (49)$$

When $M_k \geq T_k + U_k$, the partial derivative is greater than 0. It indicates that $f_{k,2}(\mathbf{P}, z_k)$ is monotonically increasing with z_k . Based on the monotonicity of $f_{k,2}(\mathbf{P}, z_k)$ and the equation (48), we can express $g_{k,2}(\mathbf{P}, v_{k,2}^*)$ in an optimization form as follows

$$g_{k,2}(\mathbf{P}, v_{k,2}^*) = \max_{z_k \leq v_{k,2}^*} f_{k,2}(\mathbf{P}, z_k) \quad (50)$$

and the Theorem 1 is proved.

APPENDIX B PROOF OF THEOREM 2

It can be seen from (30) and (32), function $\mathcal{F}_{k,2}(z_k, \mathbf{t}_k)$ ($k = 1, \dots, K$) is derived from $f_{k,2}(z_k, \mathbf{t}_k^*)$ ($k = 1, \dots, K$) by introducing a group of slack variables \mathbf{t}_k (corresponding to \mathbf{t}_k^*). Since $\log(x)$ and $-[x + \ln(1-x)]$ are monotonically increasing with x , $\mathcal{F}_{k,2}(z_k, \mathbf{t}_k)$ is thus monotonically increasing with respect to z_k and \mathbf{t}_k . Based on the fixed-point equation (23), there is an equation connection among $g_{k,2}(\mathbf{P}, v_{k,2}^*)$, $f_{k,2}(\mathbf{P}, z_k)$ and $\mathcal{F}_{k,2}(z_k, \mathbf{t}_k)$

$$\begin{aligned} g_{k,2}(\mathbf{P}, v_{k,2}^*) &= f_{k,2}(\mathbf{P}, v_{k,2}^*) \\ &= \max_{1 \leq z_k \leq v_{k,2}^*} f_{k,2}(\mathbf{P}, z_k) \\ &= \max_{1 \leq z_k \leq v_{k,2}^*} f_{k,2}(z_k, \mathbf{t}_k^*) \\ &= \max_{1 \leq z_k \leq v_{k,2}^*, \mathbf{0} \leq \mathbf{t}_k \leq \mathbf{t}_k^*} \mathcal{F}_{k,2}(z_k, \mathbf{t}_k) \end{aligned} \quad (51)$$

To simplify the constraint $z_k \leq v_{2,k}^*$, we find the fixed-point equation (23) can be also expressed in the following way

$$(v_{k,m}^*)^{-1} + \frac{1}{M_k} \sum_{n=1}^{T_k+U_k} \frac{M_k l_{m,n}^{(k,k)} P_{m,n}^{(k)}}{v_{k,m}^* \sigma_{k,m}^2(\mathbf{P}) + M_k l_{m,n}^{(k,k)} P_{m,n}^{(k)}} = 1 \quad (52)$$

where the fraction part is just right $t_{k,n}^*$ ($n = 1, \dots, T_k + U_k$) (defined in (29)). As $(v_{k,m}^*)^{-1} + \frac{1}{M_k} \sum_{n=1}^{T_k+U_k} \frac{M_k l_{m,n}^{(k,k)} P_{m,n}^{(k)}}{v_{k,m}^* \sigma_{k,m}^2(\mathbf{P}) + M_k l_{m,n}^{(k,k)} P_{m,n}^{(k)}}$ is monotonically decreasing with $v_{k,m}$, so for any $z_k \geq 0$, we have

$$\begin{aligned} z_k &\leq v_{k,2}^* \\ \Leftrightarrow (z_k)^{-1} + \frac{1}{M_k} \sum_{n=1}^{T_k+U_k} \frac{M_k l_{2,n}^{(k,k)} P_{2,n}^{(k)}}{z_k \sigma_{k,2}^2(\mathbf{P}) + M_k l_{2,n}^{(k,k)} P_{2,n}^{(k)}} &\geq 1 \\ \Leftrightarrow (z_k)^{-1} + \frac{1}{M_k} \sum_{n=1}^{T_k+U_k} t_{k,n}^* &\geq 1 \end{aligned} \quad (53)$$

By relaxing $t_{k,n}^*$ into $t_{k,n}$ ($n = 1, \dots, T_k + U_k$), the constraint $z_k \leq v_{k,2}^*$ ($k = 1, \dots, K$) can be rewritten as

$$z_k \leq v_{k,2}^* \Leftrightarrow \begin{cases} (z_k)^{-1} + \frac{1}{M_k} \sum_{n=1}^{T_k+U_k} t_{k,n} \geq 1 \\ t_{k,n} \leq t_{k,n}^*, n = 1, \dots, T_k + U_k \end{cases} \quad (54)$$

and the Theorem 2 is proved.

APPENDIX C

PROOF OF THE CONVERGENCE OF THE PROPOSED ITERATIVE ALGORITHM

By applying the Taylor expansion, the tangent of the concave function is above its curve and the tangent of the convex function is below the curve. Since $\log_2(1 - t_{k,n})$ (shown in $\mathcal{F}_{k,2}(z_k, \mathbf{t}_k)$) and z_k^{-1} are convex with respect to $t_{k,n}$ and z_k . $\ln(z_k) + \ln(t_{k,n}) + \ln(\sigma_{k,2}^2(\mathbf{P}))$ is concave with respect to $z_k, t_{k,n}$ and \mathbf{P} , the following inequalities can be easily obtained

$$\mathcal{F}_{k,2}(z_k, \mathbf{t}_k) \geq \mathcal{F}_{k,2}(z_k, \mathbf{t}_k | \mathbf{t}_k^{s-1}) \quad (55a)$$

$$\frac{1}{z_k} \geq -\frac{z_k}{(z_k^{s-1})^2} + \frac{1}{z_k^{s-1}} \quad (55b)$$

$$\begin{aligned} \ln(z_k) + \ln(t_{k,n}) + \ln(\sigma_{k,2}^2(\mathbf{P})) &\leq \\ \ln(z_k | z_k^{s-1}) + \ln(t_{k,n} | t_{k,n}^{s-1}) + \ln(\sigma_{k,2}^2(\mathbf{P} | \mathbf{P}^{s-1})) \end{aligned} \quad (55c)$$

which make the constraints (41b), (41c) and (41d) in (P6) are tighter than the corresponding constraints in (P5). Thereby, in each iteration, the optimal solution \mathbf{P}^s must be in the feasible set of the original problem.

As for the objection, since $g_{k,m,2}(\mathbf{P})$ ($m = 1, 2, k = 1, \dots, K$) is a concave function with respect to \mathbf{P} , it is easy to find that

$$g_{k,m,2}(\mathbf{P} | \mathbf{P}^{s-1}) \geq g_{k,m,2}(\mathbf{P}). \quad (56)$$

Accordingly, the following inequalities can be obtained

$$\begin{aligned} g_{k,m}(\mathbf{P}, w_{k,m}) &= g_{k,m,1}(\mathbf{P}, w_{k,m}) - g_{k,m,2}(\mathbf{P}) \\ &\geq g_{k,m,1}(\mathbf{P}, w_{k,m}) - g_{k,m,2}(\mathbf{P} | \mathbf{P}^{s-1}) \\ &= g_{k,m}(\mathbf{P}, w_{k,m} | \mathbf{P}^{s-1}). \end{aligned} \quad (57)$$

So, we have

$$g(\mathbf{P}, \mathbf{w}) \geq g(\mathbf{P}, \mathbf{w} | \mathbf{P}^{s-1}). \quad (58)$$

Furthermore, according to the properties of the saddle point, the following conclusions hold for $(\mathbf{P}^s, \mathbf{w}^s)$

$$\begin{aligned} g(\mathbf{P}^s, \mathbf{w} | \mathbf{P}^{s-1}) &\geq g(\mathbf{P}, \mathbf{w} | \mathbf{P}^{s-1}), \\ g(\mathbf{P}, \mathbf{w}^s | \mathbf{P}^{s-1}) &\leq g(\mathbf{P}, \mathbf{w} | \mathbf{P}^{s-1}). \end{aligned} \quad (59)$$

Based on (58) and (59), the relationship of $g(\mathbf{P}^s, \mathbf{w}^s)$ and $g(\mathbf{P}^{s-1}, \mathbf{w}^{s-1})$ can be derived as follows

$$\begin{aligned} g(\mathbf{P}^s, \mathbf{w}^s) &\geq g(\mathbf{P}^s, \mathbf{w}^s | \mathbf{P}^{s-1}) = \max_{\mathbf{P}} g(\mathbf{P}, \mathbf{w}^s | \mathbf{P}^{s-1}) \\ &\geq g(\mathbf{P}^{s-1}, \mathbf{w}^s | \mathbf{P}^{s-1}) = g(\mathbf{P}^{s-1}, \mathbf{w}^s) \\ &\geq \min_{\mathbf{w}} g(\mathbf{P}^{s-1}, \mathbf{w}) = g(\mathbf{P}^{s-1}, \mathbf{w}^{s-1}). \end{aligned} \quad (60)$$

The equality holds when $\mathbf{P}^s = \mathbf{P}^{s-1}, \mathbf{w}^s = \mathbf{w}^{s-1}$. Since the system has limited resources, there is an upper bound for the ergodic sum rate. Based on the monotonically increasing property of the objective function in the iterations, the convergence can be proved according to the monotonous boundary theorem.